DETERMINING RICE CROPPING PATTERNS IN TRA VINH PROVINCE USING REMOTE SENSING TIME SERIES S-1

Pham Duy Tien[1], Nguyen Thi Hong Diep[2], Duong Van Nha[3]

[1] Rural Development and Natural Resources Department, Faculty of Agriculture and Natural Resources, An Giang University, VNU-HCM

[2]Land Resources Department, College of Environment and Natural Resources, Can Tho University

[3] Kien Giang University

*Email: pdtien@agu.edu.vn

Abstracts

The study utilised farmer and field surveys, as well as time series Sentinel-1A data with a 12-day revisit time and a spatial resolution of 10 m, to detect rice cropping patterns (rice-rice-rice, other-rice-rice, fallow-rice-rice) in Tra Vinh province's three rice-growing areas. We specified the parameters determined from an agronomic perspective, as well as the related temporal features from SAR signatures, in the study to discriminate rice, other crops, and fallow land. The prediction performance of decision tree and rule-based classifiers was compared in terms of overall accuracy and kappa values. When compared to the decision tree classifier, the validation findings yielded the highest overall accuracy (86 percent). Using a rule-based approach, multitemporal Sentinel-1A imagery was used to identify rice cropping patterns at the field level with high accuracy. It was determined that the best discriminatory information for separating rice from other crops and fallow land in three consecutive seasons came from time series of co-polarized and cross-polarized polarised backscatter (VV and VH), as well as band ratio (VV/VH). When considering the major differences across crops at the crop establishment stage and its sensitivity to rice crop growth, we found that VH was the best single polarisation for classifying distinct cropping patterns. According to the study site, crop type, crop calendar, and farming methods, the parameters were appropriately set using expert knowledge and in-situ surveyed data. In the future, greater training samples may allow for more precise threshold selection. The resulting classifications map demonstrated reasonable distributions of various rice farming patterns in Tra Vinh province.

Keywords: *indices images, backscatter values, multi-temporal satellite imagery, land use/land cover types, Tra Vinh province.*

1. INTRODUCTION

Cultivated land is one of the main types of land cover and a direct carrier of food production. The change of cultivated land has a very important impact on the stability of the ecological environment and food security (Chen Hong et al., 2010; Yang Ren et al., 2013); grasp the dynamics of cultivated land The information has important reference value for crop production estimation and pricing, and the formulation of national food policies. Satellite remote sensing technology can perform earth observations at different times with different scales, different spatial resolutions, and different spectrums, and quickly obtain surface coverage data. It is a very economical and effective means for extracting cultivated land information (Hou Guanglei, etc., 2010).

The crops attached to the surface of arable land have different phenological characteristics in different seasonal phases and show different responses on the remote sensing images. it is difficult to distinguish the freshly sown or harvested arable land using single-time phase remote sensing data, and the extraction results are not highly reliable; using multi-time phase data can alleviate the above problems of single-time phase data to a certain extent, but the accuracy of extraction results is more related to how the images are selected. therefore, using time series data for arable land extraction has strong practical significance (Knight et al, 2006).

Currently, most of the studies using time series for cropland extraction are based on optical images, using the differences in vegetation reflectance at red and near-infrared wavelengths to construct vegetation indices, and extracting cropland information based on the time-domain variation of vegetation indices (e.g., ND-VI, EVI, etc.). For example, Jakubauskas

et al. (2002) performed harmonic analysis of AVHRR NDVI time series data and used the obtained amplitude and phase information to segment different crops, and Sakamoto et al. (2005) used wavelet transform to denoise and reconstruct the MODIS EVI time series data, and then determined the different fertility stages of rice by detecting the maximum, minimum, and inflection points in the time series, thus enabling dynamic monitoring of rice. The results of Wardlow et al. (2008) used a hierarchical decision tree method to process MODIS NDVI time series data to map cropping areas in the central Great Plains of the United States, and the overall accuracy of the results exceeded 80%. Victoria et al. (2012) performed Fourier transformations on MODIS NDVI data from 2006-2009 in Mato Grosso, Brazil, and then unsupervised classification of the images composed of the harmonic residuals, and finally analyzed the classification results based on spatial patterns to determine the distribution of cropland.

For optical satellites with high spatial resolution, their revisit period is relatively long and their temporal resolution is low, coupled with the influence of light and atmosphere, the available images in cloud and rain-prone areas are very limited, and the accuracy of arable land extraction is not high. Synthetic aperture radar (SAR) uses longer wavelength microwaves, and the beam can penetrate through clouds, so it can accomplish the task of earth observation regardless of light and atmospheric conditions; at the same time, SAR images also have a shorter revisit period and higher spatial resolution, and have formed a longer time series of historical observation data, which has unique advantages for farming land extraction.

In addition, due to the complexity of the SAR backscattering process with the ground surface, the intensity of backscattering is affected by internal factors such as radar wavelength, polarization mode, angle of incidence and scending/descending trajectory, as well as external factors such as vegetation biomass, vegetation canopy structure, soil water content and soil roughness (Balenzano et al, 2011); Therefore, most of the studies on arable land extraction, crop distribution and yield estimation use multi-temporal and multi-polarization SAR images to improve the accuracy of the results (Skriver et al, 2011; Tan et al, 2011; The extraction method also uses a time-vector approach, where the backscatter coefficients of all time points are considered as a multidimensional time vector, and the identification of cultivated land is converted into the classification of a multidimensional time vector (Skriver et al, 2011)

Radar backward scattering has a positive correlation with the parameters of plant height and biological volume (Chakraborty et al., 2005; Bouvet et al., 2009). The physiological parameters of plant height, vegetation coverage and biological volume are increasing and decreasing. However, due to strong speckle noise, the time curve gauge for the backward scattering coefficient of a single cultivated pixelDue to the very poor rhythm, few studies have been conducted to extract farmland using the time series change characteristics of single-band SAR data. Cheng et al. (2014) proposed a local adaptive alignment algorithm for the time series of SAR images at the pixel level. In order to investigate the applicability of SAR image time series to arable land extraction, this paper introduces the backward scattering characteristics of arable land pixels and uses thetime series similarity to extract arable land.

2. STUDY AREA AND DATA

2.1 Study area

Natural area: 2.314 km^2; the province is enclosed by Tien and Hau river with Cung Hau and Dinh An estuary. With coastline of 65 km, waterway traffic develops.

Location: The East borders East Sea; The West borders Vinh Long province; The South borders Soc Trang province; The North borders Ben Tre province. Administrative divisions: a city and 7 districts: Tra Vinh city, Cang Long, Tieu Can, Cau Ke, Tra Cu, Chau Thanh, Cau Ngang and Duyen Hai district (Figure 1).

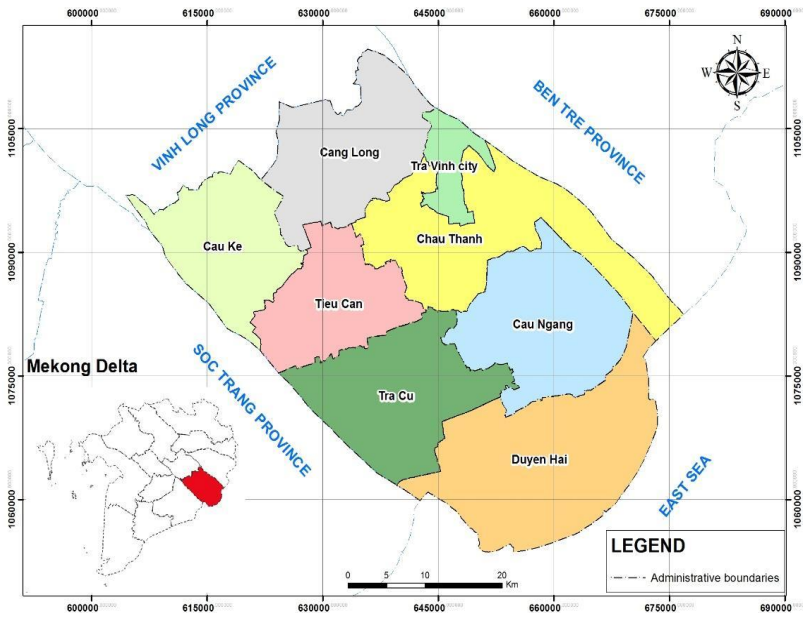

Figure 1. Administrative divisions Tra Vinh province

Farmers in Tra Vinh province may grow two to three crops each year due to the temperature, hydrology, and soil conditions, namely winter–spring (WS), summer–autumn (SA), and autumn–winter (AW) (AW). SA contributes the most rice output in Tra Vinh province among the three seasons. In some areas, during the Mua season, in which traditional rice varieties with a longer maturity period are grown, rice yields are generally low but of high quality. The major rice cropping systems are single-rice crop, double-rice crop and triple-rice crop (Table 1).

Table 1. The major rice cropping systems of Tra Vinh province (TV)

Cropping System	Seasons	Planting	Area (Units: ha)
Single-rice crop	Mua (Traditional rice)	Mua: Jul/Aug	Mua 2020: 2262.98
Double-rice crop	Dong Xuan: Winter–Spring; He Thu: Summer–Autumn	Dong Xuan: Nov–Jan; He Thu: May/Jun	Dong Xuan 2020: 60456.98 He Thu 2020: 73737.99 Thu Dong 2020: 68656.35
Triple-rice crop	Dong Xuan: Winter–Spring; He Thu: Summer–Autumn; Thu Dong: Autumn–Winter	Dong Xuan: Nov–Jan; He Thu: May/Jun; Thu Dong: Jul/Aug	

2.2 Sentinel-1 data

Sentinel-1A multi-temporal satellite SAR images were utilised to detect and map various rice-based cropping patterns. With a 12-day return duration, the Sentinel-1A mission may deliver C-band SAR data with dual polarisation capabilities (VV+VH, HH+HV), four unique imaging modes, varied resolution (down to 5 m), and coverage (up to 400km).

For this research, practically all archival Interferometric Wide Swath mode (IW) acquisitions from November 2019 to October 2020 that entirely covered the study area were made available for free. A total of 30 dual polarization (VV+VH) images with a spatial resolution of 20 m were obtained, covering the seasonal rice crop calendar (rice-rice) and growth stages over a year. Level-1 Ground Range Detected is the product kind (GRD). GRD products are created from focused SAR data that has been detected, multi-looked, and projected to the ground range using an Earth ellipsoid model such as WGS84. GRD products are made up of focussed SAR data that has been detected, multi-looked, and projected to the

ground range using an Earth ellipsoid model like WGS84. The package includes a calibration vector that allows for the straightforward conversion of image intensity measurements into sigma nought values (ESA, 2013). The normalized measure of the strength of radar signals reflected by a distributed target is the sigma nought (°), also known as the backscatter coefficient.

2.3 Field data

A field study, which included site observations and farm interviews, was carried out to aid in the interpretation of the SAR images and the validation of the classifiers. Following farm interviews of cropping methods by farmers, the goal of the sampling was to acquire field observations of rice cropping patterns practised in the surveyed sites.

The following field data was collected: (1) field corner coordinates and GPS tracks, (2) soil condition, (3) field sketch, and (4) rice plant height. Crop growth stage dates for each season were obtained through farmer interviews using a questionnaire that included questions about: (1) crop types, (2) crop number, (3) land preparation date, (4) saline intrusion date, (5) harvesting date, and (6) maturity duration.

3. RESEARCH METHODS

The main steps included field data processing, SAR data pre-processing, mean value extraction, polarization comparison and selection, non-rice area masking, parameters definition, temporal features selection, decision rules setting, classifiers validation and mapping.

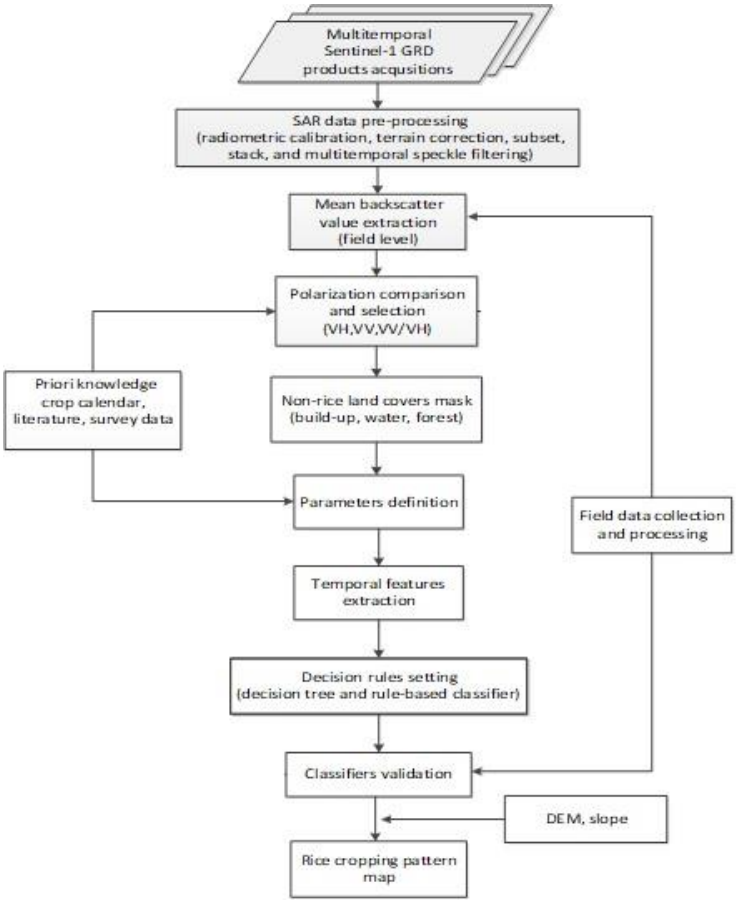

Figure 2 Methodological framework

3.1 Field data processing

We manually transcribed the questionnaire into a digital form and uploaded the GPS locations into Google Earth to digitise the rice plots to generate a viable digital field dataset. Based on field pictures and notes in the drawing, we visually removed non-rice elements such as a seedbed, trees, and a shed. Also, to confirm that the cropping pattern data gathered was typical of the research region.

3.2 Sentinel-1 data pre-processing

SAR images from Sentinel-1A IW mode were acquired over the study area (2019-2020) identify different rice cropping pattern based on a temporal analysis of the backscatter coefficient (dB). The sets of the images in GRD format were processed using the Sentinel Application Platform (SNAP) toolbox developed by ESA. It is a common software for all Sentinel images and also an ideal tool for all remote sensing image processing and analysing (L. Mansaray et al., 2017). The GRD data were transformed into a terrain geocoded backscatter coefficient by following these processing steps:
(1) Slice assembly: Slice products can be combined to form an assembled Level-1 product with the same product characteristics covering the complete segment. The operator combines overlapping products into a single composite product.
(2) Apply orbit file, radiometric calibration and terrain correction: The orbit state vectors provided in the metadata of a SAR product are generally not accurate and can be refined with the precise orbit files which are available days-to-weeks after the generation of the product. The orbit file provides accurate satellite position and velocity information. Based on this information, the orbit state vectors in the abstract metadata of the product are updated. Geometric and radiometric correction is necessary for the comparison of SAR images acquired with different sensors or acquired from the same sensor but at different times, in different modes, or processed by different processors (Lemp & Koch, 2009). Range-Doppler equations (Meier, Frei, & Nüesch, 1993) were used to transform the two-dimensional coordinates of the slant range image to three-dimensional object coordinates in a cartographic reference system. Radiometric calibration was performed using a radar equation considering the scattering area, antenna gain patterns and range spread loss (Asilo et al., 2014).
(3) Land/Sea Mask: This operation was used to create spatial or spectral subsets by either ROI (region of interest) or imported shape file.
(4) Create stacks and time-series filtering: Stack one or more slave images with respect to a master image acquired with the same observation geometry. After stacking, the multitemporal filter can reduce the speckle noise on the time-series images both in spatial and temporal dimension. Refined Lee filter was applied to the stack images as it can preserve the spatial pattern of the object and give the better crop classification accuracy (Lavreniuk et al., 2017). After these almost automatic processing steps, the corrected and normalized intensity values (DN) were generated for VH and VV separately. Then the ratio of VV and VH was created by simple band math: VV/VH (DN). The DN values were converted into backscatter coefficient (σ°) in the decibel scaling (dB) for the analysis and classification using the equation: $\sigma 0(dB) = 10 \log 10(DN)$

3.3 Polarization comparison and selection

Two different polarizations, VH and VV, and the band ratio (VV/VH) were compared based on the temporal evolution of the backscatter coefficient over the sample plots. The comparison included the following three steps:
(1) Backscatter coefficient extraction at land preparation and crop growth stages: We described the relationship among farming practice, crop calendar, and SAR acquisition timing. For each plot, based on the relation, the backscatter coefficient was selected from a single SAR acquisition that coincides with the timing of each farming event.
(2) Significance test: For rice and other crops, they had same three events: land preparation (LP), crop establishment (CE) and harvest (HA). For each of the events (LP, CE, HA), the extracted backscatter coefficients were used to calculate the significant difference between rice and others.

(3) Real rice growth cycle examination: this last step was to check the sensitivity of polarization or band ratio to the rice growth. The sensitivity was evaluated by looking at the coincidence between temporal evolution and the rice growth stages. We selected the polarization or ratio that provided the most promising significance for discriminating different crops at specific growth stages as well as representing the real rice growth cycle.

3.4. Non-rice land covers mask

Rice fields were tested to rice cropping pattern detection and classification. We created a non-rice land cover mask to reduce the possible influence of other land covers such as built-up, water, and forest on the rice signals. Throughout the year, stable water has a continuous low backscatter value. Because the transplanting phase was very temporary, it was predicted that these rice pixels would have a brief duration of low values. We excluded water bodies where the average σ° was lower than an expected threshold. Evergreen forest and built-up tend to have consistently high backscatter values throughout the year, while rice pixels tend to have high values only in a few periods, mostly prior to harvesting. We masked out forest and settlements where the average σ° was higher than an expected threshold.

4. RESULTS

4.1 Field data processing

We manually encoded the questionnaire into a digital version when the field work was completed. To ensure readability and consistency, we gave each plot a unique column name and used the same row coding style across all 100 plots. To digitize the rice plots, we uploaded the GPS locations into Google Earth and visually removed non-rice features such as seedbeds, trees, and cottages based on the notes in the sketch. The distribution of digitized plots throughout the research region is represented in Figure 3.

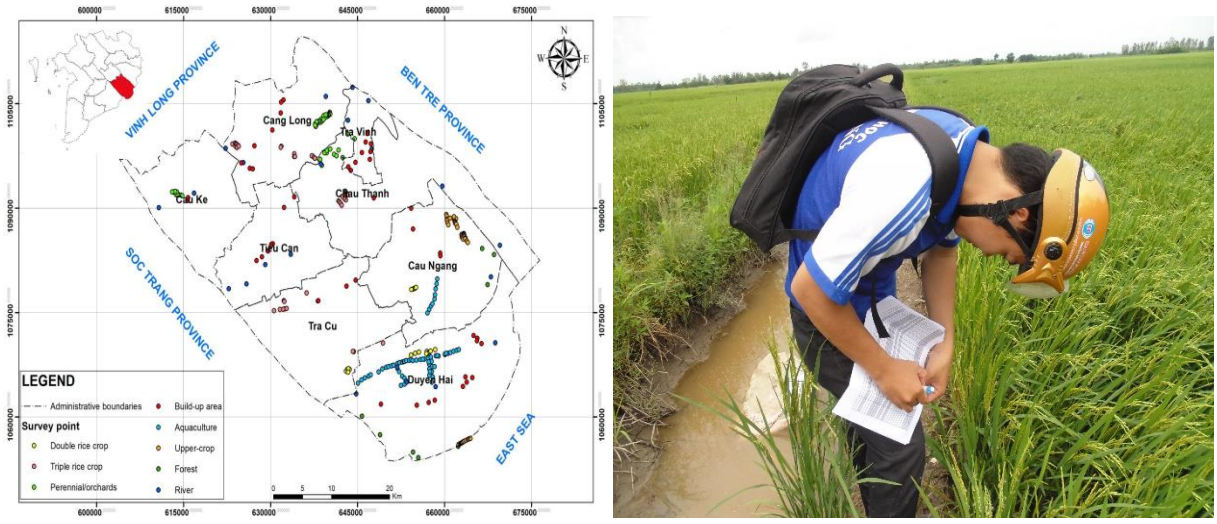

Figure 3. Distribution of visited plots across the study area

To assess the representativeness of the cropping patterns summarized from field work, we compared it with the existing survey dataset that covers the study area. We extracted 60 famers with 100 plots located in the study area and summarized the cropping pattern as shown in Table 2. From the comparison with the existing datasets, the field data matched to some extent and can be representative of the study area.

Table 2 Summary statistics of different cropping patterns.

Dry-Wet	Samples	Percentage
Rice-Rice-Rice	70	70%
Other -Rice-Rice	15	15%
Fallow-Rice-Rice	8	8%
Other patterns	7	7%
Total	100	100%

4.2 Polarization comparison and selection

In order to analyse the dry season (DS) and wet season (WS) patterns separately, the training and validation sets were divided into DS patterns and WS patterns. The number of training and validation plots for each season is shown in Table 3.

Table 3. Number of training and validation plots for DS and WS

Season	Crop or fallow	Training samples	Validation samples
DS	Rice	50	32
	Others	16	15
	Dry fallow	5	3
WS	Rice	67	47
	Wet fallow	4	3

The backscatter dynamic of one rice plot at the VH and VV polarizations of Sentinel-1A. VH polarization showed the most consistent increase in paddy rice backscatter, increasing from crop establishment to the end of reproductive phase, however, VV polarization exhibited sudden decrease from tillering to stem elongation and increase again at heading stage. Rosenthal et al. (1985) also indicated that crop biomass and height were correlated positively with C-cross (VH or HV) backscattering coefficients at high incident angles. We could consider the maximum backscattering values during the crop growth cycle as the peak of crop biomass. In summary, VH polarization showed a significant difference in land preparation and crop establishment stage as well as represented the real rice growth cycle, so we selected the VH polarization for further analysis.

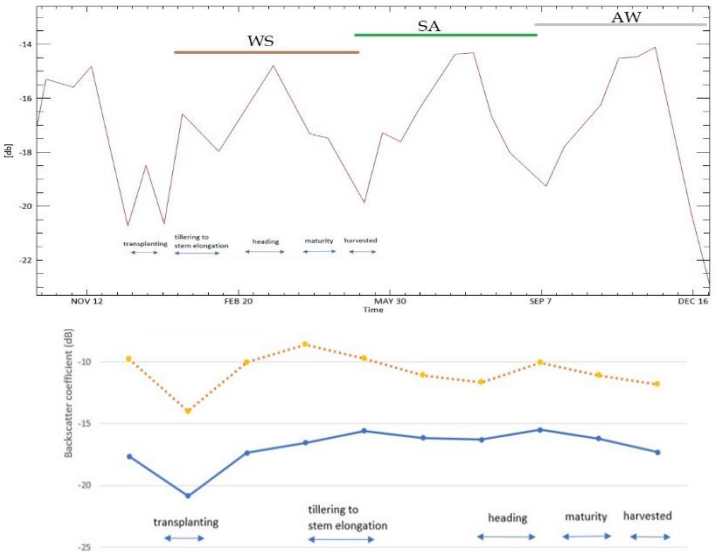

Figure 4 Backscatter dynamic of the rice plot at the VH and VV polarizations

4.3 Non-rice land covers mask

We masked out other land covers to minimize the impacts on the rice cropping patterns classification. We draw the same number of homogenous sample plots in the Google Earth for each other land cover (stable water, built-up and forest) and extracted the average dB values from the temporal signatures for each sample using the spectrum extraction tool.

Figure 5 shows the backscatter dynamic of different land covers for selected sample plots at VH polarization. Samples in DS are shown for water bodies, built-up, forest, rice, others, and dry fallow in the top portion, while water bodies, built-up, forest, rice, wet fallow in WS are shown in the lower portion.

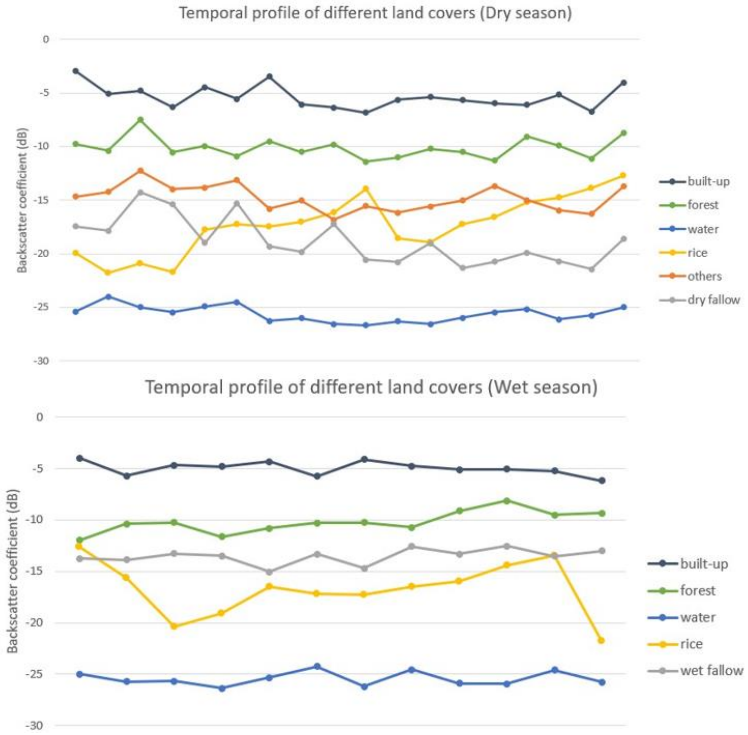

Figure 5 Backscatter dynamic of different land covers for selected ample plots in DS and WS at VH polarization

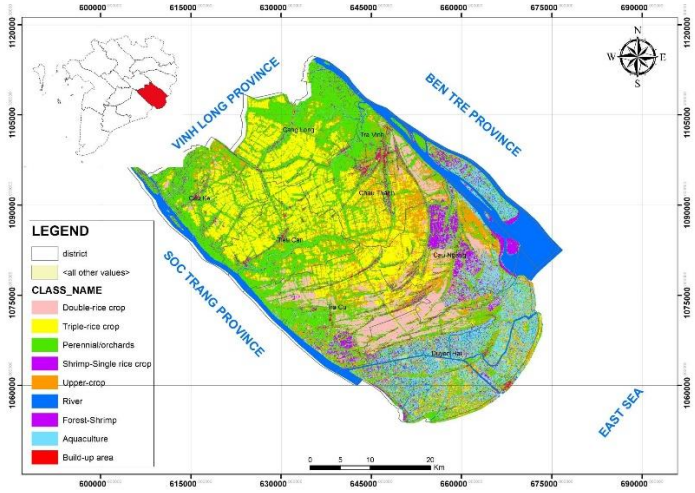

Figure 6. Land Use Land Cover Map Using SENTINEL-1 Image Series (2020)

From the above graphs, in both seasons, water bodies have a consistently very low to low dB value and urban areas showed consistently higher backscatter, whereas forest with consistently dense vegetation over time was characterized by a consistent medium to high backscatter coefficient. Rice fields were usually with water prior to crop establishment (Boschetti et al., 2014), which showed lower SAR backscatter compared to other crops, maize, for example, was not inundated at this stage (Asilo et al., 2014).

In the DS, the temporal profile of dry fallow land showed large fluctuations during the early season, and lower backscatter values in May compared to rice and other crops, while wet fallow exhibited relatively be attributed to soil moisture increase in WS. In short, stable water, built-up and forest presented distinct temporal patterns compared with different crops and fallow. Based on the temporal signatures throughout the year, we excluded water bodies where the average σ° was lower than -23 dB and masked out forest and settlement where the average σ° was higher than -14 dB.

4.4 Rice cropping pattern map

We applied the rules and thresholds in the rule-based classifier to the multitemporal σ° images to generate DS pattern and WS pattern map separately. The combination of these two consecutive maps resulted in an initial cropping pattern map (DS-WS) over one year as shown in Figure 7.

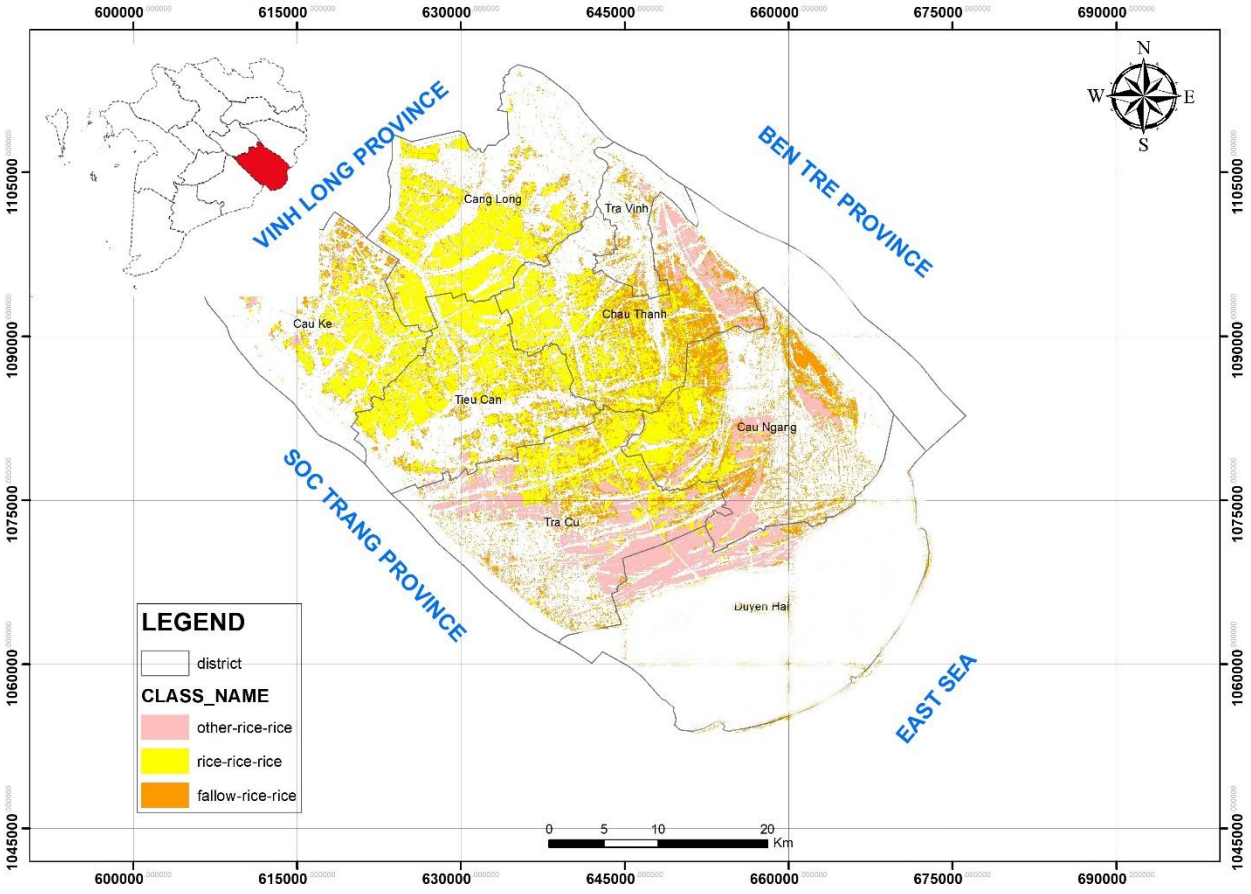

Figure 7. Rice cropping pattern obtained from rule-based classification of multitemporal Sentinel-1 images

The processing of imagery enabled the classification of the area into different rice growth stages, such as the stages in Tra Vinh province on 2020, as shown in Figure 7. The overall accuracy and Kappa coefficient of the classified result of growth stages were 86% and 0.80. To assess the ability to classify the growth stages, the differences between field data and classified results from satellite image data through the confusion matrix.

6. CONCLUSION

We specified the parameters determined from an agronomic perspective, as well as the related temporal features from SAR signatures, in the study to discriminate rice, other crops, and fallow land. In terms of total accuracy and kappa values, the prediction performance of decision tree and rule-based classifiers was evaluated. When compared to the decision tree classifier, the validation findings yielded the highest overall accuracy (86 percent). Multitemporal Sentinel-1A imagery has been utilized to delineate rice cropping patterns at the field level with excellent precision using a rule-based algorithm.

In the study, we used time series of co (VV) and cross (VH) polarized backscatter, to determine the strongest discriminatory information for distinguishing rice from other crops and fallow land across two seasons. We showed that VH was the best single polarization for classifying diverse cropping patterns, taking into account the major differences across crops at the crop establishment stage and its sensitivity to rice crop growth. Further research could look into multi-polarizations to increase classifier performance, such as introducing VV-polarized signatures at the crop establishment stage.

LIST OF REFERENCES

Chen Hong, Wu Shixin, Feng Xueli. 2010.Temporal and SpatialChanges of Cultivated Land in Xinjiang [Advance in Ear Geography, 29(3): 313-318. [Chen H, Wu SX, Feng X L. 2010. Research of changes in cultivated land in Xinji- ang based on RS and GIS[J]. Progress in Geography, 29 (3): 313-318.]

Hou Guanglei, Zhang Hongyan, Wang Yeqiao, et al. 2010. Extraction of Cultivated Land Resources in Northeast China Based on Time Series HarmonicAnalysis[J]. Journal of Natural Resources, 25(9): 1607-1617. [Hou GL, Zhang HY, Wang YQ, et al. 2010. Application of harmonic analysis of time series to extracting the crop land resource in Northeast China[J]. Journal of Natural Resources, 25(9): 1607-1617.]

Balenzano A, Mattia F, Satalino G, et al. 2011. Dense temporal series of C- and L- band SAR data for soil moisture re-trieval over agricultural crops[J]. IEEE Journal of Select- ed Topics in Applied Earth Observations and Remote Sensing, 4(2): 439-450.

Chakraborty M, Manjunath KR, Panigrahy S, et al. 2005. Rice crop parameter retrieval using multi-temporal, multi-incidence angle radarsat SAR data[J]. ISPRS Journal of Photogrammetry and Remote Sensing, 59(5): 310-322.

Jakubauskas ME, Legates DR, Kastens J H. 2002. Crop iden- tification using harmonic analysis of time- series AVHRR NDVI data[J]. Computers and Electronics in Agriculture, 37(1-3): 127-139.

Knight JF, Lunetta RS, Ediriwickrema J, et al. 2006 Region- al scale land cover characterization using MODIS- NDVI 250 m multi- temporal imagery: a phenology- based ap- proach[J]. Giscience & Remote Sensing, 43(1): 1-23.

Petitjean F, Inglada J, Gancarski P. 2012. Satellite image time series analysis under time warping[J]. IEEE Transactions on Geoscience and Remote Sensing, 50(8): 3081-3095.

Sakamoto T, Yokozawa M, Toritani H, et al. 2005. A crop phe- nology detection method using time- series MODIS data [J]. Remote Sensing of Environment, 96(3-4): 366-374.

Skriver H, Mattia F, Satalino G, et al. 2011. Crop classification using short-revisit multitemporal SAR data[J]. IEEE Jurnal of Selected Topics in Applied Earth Observations and Remote Sensing, 4(2): 423-431.

Victoria DD, Da Paz AR, Coutinho AC, et al. 2012 Crop- land area estimates using MODIS NDVI time series in the state of Mato Grosso, Brazil[J]. Pesquisa Agropecuar- ia Brasileira, 47(9): 1270-1278.

Wardlow BD, Egbert S L. 2008. Large-area crop mapping us- ing time-series MODIS 250 m NDVI data: an assessment for the US central great plains[J]. Remote Sensing of En- vironment, 112(3): 1096-1116.

Asilo, S., de Bie, K., Skidmore, A., Nelson, A., Barbieri, M., & Maunahan, A. (2014). Complementarity of t wo rice mapping approaches: Characterizing strata mapped by hypertemporal MODIS and rice padd y identification using multitemporal SAR. Remote Sensing, 6(12), 12789–12814. https://doi.org/10.339 0/rs61212789

Boschetti, M., Nutini, F., Manfron, G., Brivio, P. A., & Nelson, A. (2014). Comparative Analysis of Norm alised Difference Spectral Indices Derived from MODIS for Detecting Surface Water in Flooded Ric e Cropping Systems. PLoS

ONE, 9(2), e88741. https://doi.org/10.1371/journal.pone.0088741

ESA. (2013). Sentinel-1 user handbook. European Space Agency technical note. https://doi.org/10.1017/CBO9781107415324.004

Lavreniuk, M., Kussul, N., Meretsky, M., Lukin, V., Abramov, S., & Rubel, O. (2017). Impact of SAR Dat a Filtering on Crop Classification Accuracy. IEEE First Ukraine Conference on Electrical and Computer En gineering (UKRCON), 912–916. https://doi.org/10.1109/UKRCON.2017.8100381

Lemp, D., & Koch, B. (2009). Forest monitoring using TerraSAR-X data—evaluation of processing meth ods and first results. Proceedings of TerraSAR-X Science Meeting, (March 2014). Retrieved from https://www.researchgate.net/publication/260920517

Mansaray, L., Huang, W., Zhang, D., Huang, J., & Li, J. (2017). Mapping Rice Fields in Urban Shanghai, S outheast China, Using Sentinel-1A and Landsat 8 Datasets. Remote Sensing, 9(3), 257. https://doi.org/ 10.3390/rs9030257

Mansaray, L. R., Zhang, D., Zhou, Z., & Huang, J. (2017). Evaluating the potential of temporal Sentinel-1 A data for paddy rice discrimination at local scales. Remote Sensing Letters, 8(10), 967–976. https://doi.org/10.1080/2150704X.2017.1331472